RSC Advances

PAPER

View Article Online
View Journal | View Issue

Cite this: *RSC Adv.*, 2023, **13**, 17097

Packing bimodal magnetic particles to fabricate highly dense anisotropic rare earth bonded permanent magnets

Xubo B. Liu, [a] Kinjal Gandha, [a] Haobo Wang,[b] Kaustubh Mungale, [cde] Uday Kumar Vaidya,[cde] Ikenna C. Nlebedim *[a] and Mariappan Parans Paranthaman *[b]

Highly dense and magnetically anisotropic rare earth bonded magnets have been fabricated *via* packing bimodal magnetic particles using a batch extrusion process followed by compression molding technology. The bimodal feedstock was a 96 wt% magnet powder mixture, with 40% being anisotropic Sm-Fe-N (3 μm) and 60% being anisotropic Nd-Fe-B (100 μm) as fine and coarse particles, respectively; these were blended with a 4 wt% polyphenylene sulfide (PPS) polymer binder to fabricate the bonded magnets. The hybrid bonded magnet with an 81 vol% magnet loading yielded a density of 6.15 g cm^{-3} and a maximum energy product $(BH)_m$ of 20.0 MGOe at 300 K. Scanning electron microscopy (SEM) indicated that the fine-sized Sm-Fe-N particles filled the gap between the large Nd-Fe-B particles. Rietveld analysis of the X-ray diffraction data showed that the relative contents of the $Nd_2Fe_{14}B$ and $Sm_2Fe_{17}N_3$ phases were 61% and 39%, respectively, in the hybrid bonded magnet. The PPS binder coated most of the magnetic particles homogeneously. Compared with the magnetic properties of the initial Nd-Fe-B and Sm-Fe-N powders, the reduction in the remanence, from the demagnetization curve, is ascribed to the dilution effect of the binder, the non-perfect alignment, and the internal magnetic stray field.

Received 10th April 2023
Accepted 25th May 2023

DOI: 10.1039/d3ra02349d

rsc.li/rsc-advances

1. Introduction

Rare earth permanent magnets such as Nd-Fe-B, have been widely used in electric/hybrid vehicles, wind generators and other consumer electronic devices.[1–3] The full-density (7.6 g cm^{-3}) sintered or hot-deformed Nd-Fe-B magnets have a maximum energy product (BH_m) in the range of 50–55 MGOe but are mechanically brittle and it is difficult to make components with complex shapes and small sizes. On the other hand, Nd-Fe-B bonded magnets have better mechanical properties and can be made into magnetic components with a near-net shape, although their energy product is low.[4] Conventionally, bonded magnets are fabricated by injection molding and compression molding and have a typical magnet powder loading fraction between 65 and 80 vol%, respectively.[5] Additive manufacturing (AM) is becoming a promising technique for bonded permanent magnet (PM) production.[6–14] Compared to the conventional subtractive methods of manufacturing, AM has the advantage of components being formed into the net shape without the requirement of special tools and the critical rare earth raw materials are not wasted.

Besides the extrinsic magnetic properties of the magnet powder itself, the magnetic performance of an anisotropic bonded magnet depends on the volume fraction and the alignment of the easy magnetization directions of the particles. In our previous work,[15] we have shown that the magnetic alignment of particles depends on the filling fraction of the magnetic powder, binder type and magnetic field to align the particles during processing. Depending on the particle loading fraction and the rheological state of the binder during magnetic alignment, a magnetic field strength of ≥1.5 T is enough to gain high magnetic alignment of anisotropic Nd-Fe-B bonded magnets with either nylon-12 or polyphenylene sulfide (PPS) as the binder. One way to increase the powder filling fraction is to reduce the content of the binder. However, a minimum content of the binder is required to maintain sufficient mechanical strength in the final products. For a fixed binder content, maximizing the filling fraction of magnetic powder is a great challenge. It is well known that particles of the same size can provide a close-packed arrangement, providing 74% packing by volume, while the same set of spheres in random closed-packing offers about 63% space filling.[16] However, in practice, the arrangement is not close-

[a]*Critical Materials Institute, Ames Laboratory, Ames, IA 50010, USA. E-mail: nlebedim@ameslab.gov*

[b]*Chemical Sciences Division, Oak Ridge National Laboratory, Oak Ridge, TN 37831, USA. E-mail: paranthamanm@ornl.gov*

[c]*Tickle College of Engineering, The University of Tennessee, Middle Drive, Knoxville, TN 37996, USA*

[d]*Manufacturing Sciences Division, Oak Ridge National Laboratory, 2350 Cherahala Blvd, Knoxville, TN 37932, USA*

[e]*Institute for Advanced Composites Manufacturing Innovation, 2360 Cherahala Blvd, Knoxville, TN 37932, USA*

packed, and all particles are not the same size. Tailoring the feedstock powder parameters such as particle size distribution and shape can help develop high-quality additively manufactured bonded magnets. The shape of the magnetic powder is limited by the chosen manufacturing methods. Another way to increase the volume fraction of the magnetic powder is the adoption of feedstock powder with a bimodal size distribution, *i.e.*, tailoring the ratio between fine and coarse particles in the feedstock powder.[17] If the particle diameter ratio between fine and coarse particles is greater than 10, the fine particles will mostly enter the gaps between the coarse particles to improve the particle packing fraction based on the Furnas model. Ideally, we would use the same type of coarse and fine particles such as Nd-Fe-B or Sm-Fe-N to investigate the bimodal size effect. The commercial anisotropic Nd-Fe-B powders used for fabricating bonded magnets such as MQA and Magfine have typical particle sizes of several tens to several hundred micrometers. Unfortunately, MQA or Magfine Nd-Fe-B powder will lose coercivity and also magnet powder becomes very reactive in air when the powder size is reduced to several micrometers.[18–20] On the other hand, Sm-Fe-N powder can achieve high coercivity with a particle size of less than several micrometres.[21–24] The varied dependence of coercivity on particle size is related to the different coercivity mechanisms.[25,26] Hence, it is almost impossible to use either fine Nd-Fe-B or coarse Sm-Fe-N powder for producing bonded magnets. However, it is easy to prepare bimodal bonded magnets with Nd-Fe-B and Sm-Fe-N as coarse and fine particle feedstocks, respectively.

Several hybrid bonded magnets exist for other purposes. The hybrid bonded magnet is composed of two or more different types of magnetic powder to achieve a predefined target performance such as maximum energy product or thermal stability, *etc.*[27–32] For example, the Nd-Fe-B/ferrite hybrid bonded magnet shows magnetic properties that are lower as compared to Nd-Fe-B but better than that of ferrite magnets.[27,29] However, the Nd-Fe-B/Sm-Fe-N hybrid magnets have thermal stability with magnetic properties that are better than those of Nd-Fe-B bonded magnets.[30] This provides additional choices for making bimodal bonded magnets to achieve the large volume fraction filling of magnetic particles and high magnetic performance. Sm-Fe-N powder has a typical particle size of several micrometers and similar magnetic properties to Nd-Fe-B, which can function as fine particles in the preparation of hybrid bonded magnets. Optimized processing conditions are needed to pack the particles of the highly dense bonded magnets by using polymer binders such as PPS, nylon, or epoxy resin. The processing includes the following: (1) the magnetic powder and binder are blended, and each magnetic powder is coated with the binder to obtain the compounded pellets; (2) there are several methods for packing the composite powders to fabricate bonded magnets such as compression molding, injection molding, additive manufacturing, *etc.*

We have designed and fabricated bonded magnets with bimodal-sized magnetic powders as feedstock *via* compounding with a batch mixer followed by compression molding. Here, the Magfine anisotropic Nd-Fe-B powder and Sm-Fe-N were selected as coarse and fine particles to maximize the filling fraction of the magnetic powder and the magnetic performance of the bonded magnets. The microstructure and magnetic properties have been characterized by X-ray powder diffraction (XRD), scanning electron microscopy (SEM) and magnetic property measurements. We have also discussed the potential pathways to further improve the performance of anisotropic Nd-Fe-B/Sm-Fe-N hybrid bonded magnets prepared using bimodal-sized magnetic particles as the feedstock powder for additive manufacturing.

2. Experimental methods

We selected the anisotropic Nd-Fe-B (Magfine) powder and Nd-Fe-B + Sm-Fe-N + polyphenylene sulfide (PPS) pellets (Magfine MF15P) as feedstock for preparing bonded magnets using compression molding. To achieve the optimized magnetic performance, we controlled the ratios of the coarse NdFeB powder and fine SmFeN powder, the content of the binder, and the processing conditions. The ratio of NdFeB to SmFeB was selected as 3 : 2 based on the initial packing. The PPS content was reduced to 4 wt% to increase the relative fraction of magnetic powder. *i.e.*, the composite pellets with a mixture of 96 wt% magnetic powder (*i.e.*, a mixture of 60% anisotropic Nd-Fe-B and 40% anisotropic Sm-Fe-N) in 4 wt% PPS binder. To ensure the homogeneous coating of binder on the magnetic particle surface with low binder content, we blended the magnetic powder and PPS using a Brabender batch mixer and extruded the pellet using a Berstorff twin screw extruder. The extruded pellets were hot-pressed using a 30 ton Carver hydraulic press at a temperature of 200 °C to achieve high density. The details of extrusion and compression molding conditions have been published earlier.[33]

The commercial Magfine MF15P composite magnet has a magnetic remanence B_r of 13.2 kGs, a coercivity H_{ci} of 14 kOe and a maximum energy product $(BH)_{max}$ of 41 MGOe. The MF15P powder has an average particle size of 100 μm. The Sm-Fe-N anisotropy magnetic powder has an average particle size of 3 μm with magnetic properties of $B_r = 13$ kGs, $H_{ci} = 10$ kOe and $BH_m = 36$ MGOe. No (or negligible) kinks were expected in the demagnetization curves of the hybrid bonded magnet due to the similar magnetic properties of these two kinds of powder. The big particle size difference meets the requirement for bimodal close packing conditions as discussed above. Given that there is porosity in a conventional bonded magnet, the actual volume fraction of magnetic particles ($V_{particle}$) in hybrid bonded magnets can be estimated based on the density of bonded magnets (ρ_m) and magnetic particles (ρ_i), and the mass fraction of magnetic particles (M_i), *i.e.*, as shown in formula (1):

$$V_{particle} = \rho_m \sum_{i=1}^{n} \frac{M_i}{\rho_i} \quad (1)$$

The melting point of the binder in the bonded magnet was determined *via* Differential Scanning Calorimetry (DSC) measurements using a NETZSCH STA449F3 Jupiter thermal analyzer. The melting point was about 560 K, slightly higher than that of pure PPS (553 K). The magnetic alignment was achieved

through magnetic field annealing under an applied external magnetic field of 1.5 T at a temperature of 590 K. The magnetically aligned bonded magnets were tested in a Quantum Design MPMS-3 Vibration Sample Magnetometer (VSM) at 300 K. The microstructures of the bonded magnets were observed using a Field-Emission Scanning Electron Microscope (FE-SEM, FEI Teneo). XRD data were collected using a PANalytical X'Pert PRO diffractometer with Co K_α radiation. Rietveld analysis of the XRD data was performed using the GSAS-II package.[34]

3. Results and discussion

3.1. The design and fabrication of bonded magnets with bimodal magnetic particles

When monodisperse spheres are transferred into a container and tapped or vibrated to cause them to settle, they are observed experimentally to achieve packing densities of between 0.60 and 0.64, which is typical for the random closed packing situation.[35] For the bimodal packing of very large coarse particles with very small fine particles (the diameter ratio is higher than 10), the fully dense, coarse particles replace the space occupied by the fine particles and the associated pore volume to improve the filling fraction. This can also be understood as the fine particles occupying the pores between coarse particles to maximize the total filling fraction of particles. The commercial Nd-Fe-B anisotropic powder for the bonded magnet (Magfine), prepared by the HDDR (Hydrogenation-Disproportionation-Desorption-Recombination) process, has a typical particle size of 100 μm. The Sm-Fe-N anisotropic powder has a typical particle size of 3 μm and comparable magnetic properties (36 MGOe) as those of Magfine Nd-Fe-B particles (41 MGOe). As a starting point, we selected 60% of coarse particles (Nd-Fe-B) and 40% of fine particles (Sm-Fe-N) as the feedstock magnetic powder for compression molding to study the effects of bimodal-sized particles on the filling fraction and magnetic properties.

The as-fabricated bonded magnet has a density of 6.15 g cm^{-3}. Based on the formula (1), the estimated volume filling fraction is 0.81 for magnetic particles (Nd-Fe-B + Sm-Fe-N), which is much higher than the theoretical maximum value of close-packed mono-sized particles (0.74). We ascribe the high filling fraction to the bimodal particle packing effect, as schematically shown in Fig. 1. The fine Sm-Fe-N particles occupy the gap between the large Nd-Fe-B particles and increase the total filling fraction of magnetic powder and reduce the porosity. This agrees with the random close-packing model of particles as discussed above.

We performed SEM and XRD analyses on the bonded magnets to gain more insight into the bimodal particle distribution. As shown in Fig. 2, the fine-sized Sm-Fe-N particles are well mixed with the binder (PPS) and distributed between large Nd-Fe-B particles. However, further increasing the homogenous distribution of fine particles may improve the filling fraction of magnetic particles.

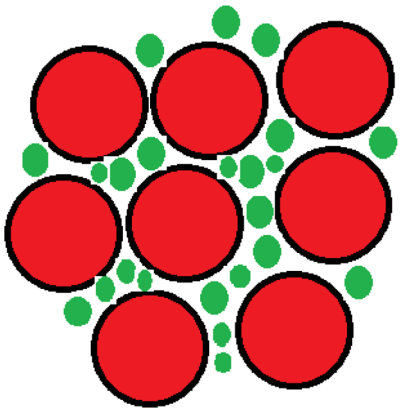

Fig. 1 Scheme of bimodal particle packing to improve the packing fraction.

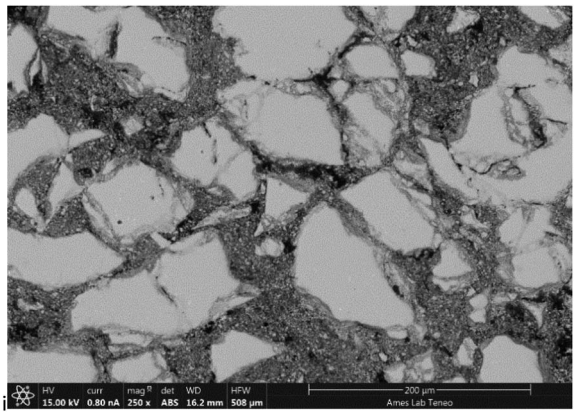

Fig. 2 SEM of the Nd-Fe-B/Sm-Fe-N hybrid bonded magnet. The large Nd-Fe-B particles are surrounded by fine Sm-Fe-N powder.

Fig. 3 displays the XRD of the Nd-Fe-B/Sm-Fe-N hybrid bonded magnet with a bimodal particle size distribution. The XRD patterns are dominated by the contributions from the $Nd_2Fe_{14}B$ and $Sm_2Fe_{17}N_3$ phases beside minor peaks from PPS. In the quantitative XRD fitting, the minor peaks such as those from Nd-rich phases and those from partially crystallized PPS are buried in the background and are not included. The Rietveld fitting indicates the presence of 61% of the $Nd_2Fe_{14}B$ phase and 39% of the $Sm_2Fe_{17}N_3$ phase in the sample (Table 1), which agrees with our targeted values, as described in the

Table 1 XRD Rietveld-fitted results of the Nd-Fe-B/Sm-Fe-N hybrid bonded magnet. (wR = 2.22%, R = 1.71%, GOF = 1.4)

Phase	Space group	Lattice constant a (Å)	Lattice constant c (Å)	Content (vol%)
$Nd_2Fe_{14}B$	$P4_2/mnm$	8.7987(2)	12.2108(4)	61
$Sm_2Fe_{17}N_3$	R-3M	8.7373(5)	12.6568(6)	39

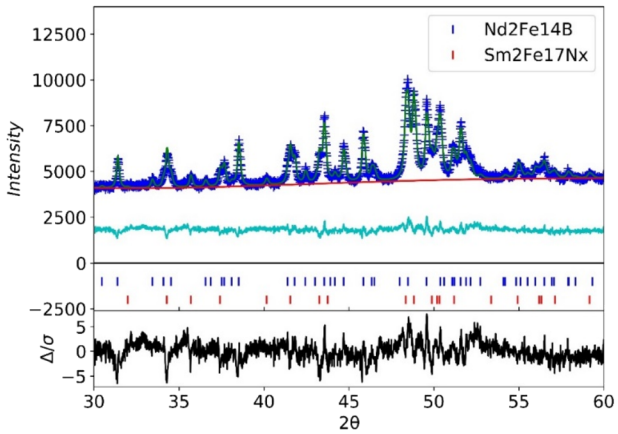

Fig. 3 Experimental (blue crossing) and fitted (green line) XRD diffraction patterns of the Nd-Fe-B/Sm-Fe-N hybrid bonded magnet.

Experimental section. The fitted lattice constants are in good agreement with the previously reported values.[36,37]

3.2. Magnetic properties of the hybrid bonded magnet with post-magnetic field alignment

The magnetic particles were aligned using post-compression annealing of the as-compressed Nd-Fe-B/Sm-Fe-N bonded magnet under the magnetic field (see details in Section 2). Fig. 4 displays the magnetic hysteresis of the post-magnetic field annealed Nd-Fe-B/Sm-Fe-N bonded magnet. The hybrid bonded magnet shows excellent magnetic properties of a B_r of 10.4 kG, a H_{ci} of 10.8 kOe, and a $(BH)_{max}$ of 20 MGOe at 300 K. The high magnetic performances are ascribed to the high filling fraction of the magnetic powder. The remanence B_r is directly proportional to the filling fraction while the maximum energy product $(BH)_m$ increases parabolically with B_r or the filling fraction. If we consider the dilution effect in the bonded magnet due to the binder (PPS), the expected B_r value should be 10.8 kGs, which is higher than the experimentally obtained value by about 3.5%. The slightly reduced B_r value may be related to the possible non-perfect magnetic alignment and the inter-particle static magnetic interaction. Both the non-aligned particle and the internal magnetic stray field will reduce the B_r and H_{ci} values. The H_{ci} value obtained for the bonded magnet (10.8 kOe) is slightly higher than that of Sm-Fe-N (10.0 kOe), but less than that of Nd-Fe-B powder (14 kOe), resulting from the linear overlapping effect and the internal magnetic stray field in the hybrid magnet.

To evaluate the homogeneous performance of the magnetic properties of the bonded magnets, we chose three pieces for the VSM measurements. As shown in Table 2, the fluctuations of B_r, H_{ci} and BH_m were less than 2%, 0.5% and 3%, respectively.

In this work, we selected the coarse- (60% Nd-Fe-B) and fine-particle (40% Sm-Fe-N) ratios based on the assumption that the mono-sized coarse powder Nd-Fe-B and fine-particle Sm-Fe-N were mixed to maximize the filling fraction of magnetic powder in the compression-bonded magnet technology. However, the particle size distribution of Nd-Fe-B and Sm-Fe-N

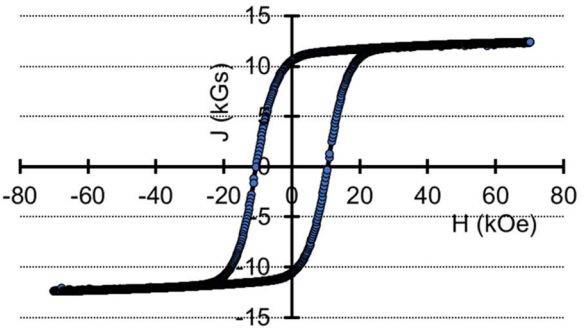

Fig. 4 Magnetic hysteresis loop J–H of the Nd-Fe-B/Sm-Fe-N hybrid bonded magnet.

Table 2 Magnetic properties of the Nd-Fe-B/Sm-Fe-N hybrid magnet

Sample ID	Remanence B_r (kGs)	Coercivity H_{ci} (kOe)	Maximum energy Product $(BH)_m$ (MGOe)
1	10.4	10.80	20.0
2	10.5	10.82	20.0
3	10.2	10.76	19.5

powder also plays an important role. As a future study, we will investigate the effects of different particle size distributions and the volume ratio between Nd-Fe-B and Sm-Fe-N powders on the filling fraction and magnetic properties of the hybrid bonded magnets to further optimize the magnetic performance of the bonded magnet prepared by additive manufacturing.

4. Conclusions

We have demonstrated bimodal-sized coarse particles (Nd-Fe-B) and fine powders (Sm-Fe-N) for successfully increasing the filling fraction of the magnetic powder in hybrid bonded magnets prepared by an extrusion process followed by compression molding. The obtained bonded magnet achieved a maximum energy product of 20 MGOe, which is much better than the conventional injection-molded bonded magnets. This work indicates that the proposed manufacturing method can be transferred to an additive manufacturing compression molding process, which is an effective and competitive method for fabricating high-performance bonded magnets.

Author contributions

Conceptualization, XBL, ICN, MPP; methodology, XBL, KG, HW, KM; formal analysis, XBL, KG, KM, ICN, MPP; writing – original draft preparation, XBL, KG, HW, KM; writing – review & editing, UKV, ICN, MPP; supervision, UKV, ICN, MPP; funding acquisition, ICN, MPP.

Conflicts of interest

There are no conflicts to declare.

Acknowledgements

This work is supported by the Critical Materials Institute (CMI), an Energy Innovation Hub funded by the U.S. Department of Energy (DOE), Office of Energy Efficiency and Renewable Energy, Advanced Materials and Manufacturing Technologies Office. All the electron microscopy work was performed in the Sensitive Instrument Facility at Ames Laboratory, which is operated for the U.S. Department of Energy by Iowa State University of Science and Technology under Contract No. DE-AC02-07CH11358. Part of the development of critical rare earth free magnet research was supported by the U.S. Department of Energy, Office of Energy Efficiency and Renewable Energy, Wind Energy Technologies Office Program. This manuscript has been authored in part by UT-Battelle, LLC, under contract DE-AC05-00OR22725 with the US Department of Energy (DOE). The US government retains and the publisher, by accepting the article for publication, acknowledges that the US government retains a nonexclusive, paid-up, irrevocable, worldwide license to publish or reproduce the published form of this manuscript, or allow others to do so, for US government purposes. DOE will provide public access to these results of federally sponsored research in accordance with the DOE Public Access Plan (**http://energy.gov/downloads/doe-public-access-plan**).

References

1 M. Sagawa, S. Fujimura, H. Yamamoto and Y. Matsuura, *IEEE Trans. Magn.*, 1984, **20**, 1584–1589.
2 J. J. Croat, J. F. Herbst, R. W. Lee and F. E. Pinkerton, *J. Appl. Phys.*, 1984, **55**, 2078–2082.
3 O. Gutfleisch, M. A. Willard, E. Brück, C. H. Chen, S. G. Sankar and J. P. Liu, *Adv. Mater.*, 2011, **23**, 821–842.
4 J. Ormerod and S. Constantinides, *J. Appl. Phys.*, 1997, **81**, 4818–4820.
5 B. M. Ma, J. W. Herchenroeder, B. Smith, M. Suda, D. Brown and Z. Chen, *J. Magn. Magn. Mater.*, 2002, **239**, 418–423.
6 M. P. Paranthaman, C. S. Shafer, A. M. Elliott, D. H. Siddel, M. A. McGuire, R. M. Springfield, J. Martin, R. Fredette and J. Ormerod, *J. Met.*, 2016, **68**, 1978–1982.
7 L. Li, A. Tirado, B. S. Conner, M. Chi, A. M. Elliott, O. Rios, H. Zhou and M. P. Paranthaman, *J. Magn. Magn. Mater.*, 2017, **438**, 163–167.
8 L. Li, A. Tirado, I. C. Nlebedim, O. Rios, B. Post, V. Kunc, R. R. Lowden, E. Lara-Curzio, R. Fredette, J. Ormerod, T. A. Lograsso and M. P. Paranthaman, *Sci. Rep.*, 2016, **6**, 36212.
9 C. Huber, C. Abert, F. Bruckner, M. Groenefeld, S. Schuschnigg, I. Teliban, C. Vogler, G. Wautischer, R. Windl and D. Suess, *Sci. Rep.*, 2017, **7**, 9419.
10 K. von Petersdorff-Campen, Y. Hauswirth, J. Carpenter, A. Hagmann, S. Boës, M. S. Daners, D. Penner and M. Meboldt, *Appl. Sci.*, 2018, **8**, 1275.
11 J. Jaćimović, F. Binda, L. G. Herrmann, F. Greuter, J. Genta, M. Calvo, T. Tomše and R. A. Simon, *Adv. Eng. Mater.*, 2017, **19**, 1700098.
12 A. B. Baldissera, P. Pavez, P. A. P. Wendhausen, C. H. Ahrens and J. M. Mascheroni, *IEEE Trans. Magn.*, 2017, **53**, 1–4.
13 P. P. Wendhausen, C. H. Ahrens, A. B. Baldissera, P. D. Pavez and J. M. Mascheroni, in *2017 IEEE International Magnetics Conference, INTERMAG 2017*, 2017.
14 K. Gandha, I. C. Nlebedim, V. Kunc, E. Lara-Curzio, R. Fredette and M. P. Paranthaman, *Scr. Mater.*, 2020, **183**, 91–95.
15 X. B. Liu, K. Gandha, I. C. Nlebedim and M. P. Paranthaman, *J. Phys. D: Appl. Phys.*, 2021, **54**, 315004.
16 S. Torquato, T. M. Truskett and P. G. Debenedetti, *Phys. Rev. Lett.*, 2000, **84**, 2064.
17 H. Y. Sohn and C. Moreland, *Can. J. Chem. Eng.*, 1968, **46**, 162–167.
18 K. Noguchi, C. Mishima, M. Yamazaki, H. Matsuoka, H. Mitarai and Y. Honkura, *1st International Electric Drives Production Conference 2011, EDPC-2011 – Proceedings*, 2011, pp. 181–186.
19 Y. Nozawa, K. Iwasaki, S. Tanigawa, M. Tokunaga and H. Harada, *J. Appl. Phys.*, 1988, **64**, 5285–5289.
20 X. Liu, Y. Xiao, Z. Zhang, B. Qiu and R. Wang, *Chin. J. Eng.*, 1999, **21**(5), 462–464.
21 Y. Otani, D. P. F. Hurley, H. Sun and J. M. D. Coey, *J. Appl. Phys.*, 1991, **69**, 5584–5589.
22 Y. Hirayama, A. K. Panda, T. Ohkubo and K. Hono, *Scr. Mater.*, 2016, **120**, 27–30.
23 K. Kobayashi, R. Skomski and J. M. D. Coey, *J. Alloys Compd.*, 1995, **222**, 1–7.
24 R. Arlot, H. Izumi, K. Machida, D. Fruchart and G. Adachi, *J. Magn. Magn. Mater.*, 1997, **172**, 119–127.
25 Y. Ming, L. Xubo, Y. Xiao and Z. Jiuxing, *J. Magn. Magn. Mater.*, 2004, **269**, 227–230.
26 J. Ding, R. Street and P. G. McCormick, *J. Magn. Magn. Mater.*, 1992, **115**, 211–216.
27 J. Schneider and R. Knehans-Schmidt, *J. Magn. Magn. Mater.*, 1996, **157–158**, 27–28.
28 J. Tian, Z. Tang, Z. Zuo, D. Pan and S. Zhang, *Mater. Lett.*, 2013, **105**, 87–89.
29 X.-C. Zhong, G. Hu, X.-J. Guo and Z.-W. Liu, *J. Mater. Eng.*, 2016, **44**, 9–13.
30 K. Gandha, L. Li, I. C. Nlebedim, B. K. Post, V. Kunc, B. C. Sales, J. Bell and M. P. Paranthaman, *J. Magn. Magn. Mater.*, 2018, **467**, 8–13.
31 B. Ma, A. Sun, X. Gao, X. Bao, J. Li and H. Lang, *J. Magn. Magn. Mater.*, 2018, **457**, 70–74.
32 H. Fukunaga, H. Murata, T. Yanai, M. Nakano and F. Yamashita, *J. Appl. Phys.*, 2010, **107**, 09A736.
33 K. Mungale, T. N. Lamichhane, H. Wang, B. C. Sales, M. P. Paranthaman and U. K. Vaidya, *Materialia*, 2021, **19**, 101167.
34 B. H. Toby and R. B. Von Dreele, *J. Appl. Crystallogr.*, 2013, **46**, 544–549.
35 G. D. Scott and D. M. Kilgour, *J. Phys. D: Appl. Phys.*, 1969, **2**, 311.
36 J. M. D. Coey and H. Sun, *J. Magn. Magn. Mater.*, 1990, **87**, L251–L254.
37 J. F. Herbst, *Rev. Mod. Phys.*, 1991, **63**, 819–898.